PAPER

Aggregation and dendritic growth in a magnetic granular system

Journal of Statistical Mechanics: Theory and Experiment
An IOP and SISSA journal

Aggregation and dendritic growth in a magnetic granular system

J González-Gutiérrez[1], J L Carrillo-Estrada[1] and J C Ruiz-Suárez[2]

[1] Instituto de Física, Benemérita Universidad Autónoma de Puebla, A. P. J-48, Puebla 72570, Mexico
[2] CINVESTAV-Monterrey, PIIT, Nuevo León, 66600, Mexico
E-mail: jorgegg@ifuap.buap.mx, carrillo@ifuap.buap.mx and jcrs.mty@gmail.com

Received 18 October 2013
Accepted for publication 27 November 2013
Published 20 December 2013

Online at stacks.iop.org/JSTAT/2013/P12015
doi:10.1088/1742-5468/2013/12/P12015

Abstract. We experimentally study the aggregation of non-Brownian paramagnetic beads in a vibrofluidized system induced by an external magnetic dipole. A dendritic growth is observed in real time, particle by particle, and with the naked eye. Two aggregation stages are observed, where tip, tip-split and side-branching growths are differentiated. We found clusters morphologically similar to those generated by a diffusion limited aggregation algorithm (DLA). However, in our case, due to the finite range of the magnetic field, the clusters reach a finite size and their structures exhibit different rates of aggregation. These are revealed by the existence of two different scaling relations of the mass with the gyration radius, and the nature of the radial mass distribution function. The structures of the clusters are fractal objects with an effective mass fractal dimension of around 1.8. We found that an exponential function describes the aggregation phenomenon as a function of time. This exponential behavior is independent of the final state of the morphology (shape and length) of the agglomerates.

Keywords: granular matter, cluster aggregation (experiment), dendritic growth (experiment)

1742-5468/13/P12015+13$33.00

Contents

1. Introduction

The omnipresence of aggregation processes in Nature has motivated a great deal of research in recent decades [1, 2]. However, while a vast amount of knowledge has been so far accumulated, there are unanswered questions. The presence of asymmetric interaction potentials and entropic forces, for example, that under certain conditions generate self-assembled complex structures that preserve some track of the interactions that drive the aggregation, is not well understood. A dendritic body is an example of a fractal pattern self-assembled by a random and sometimes complex dynamics. The geometry of such structures appears as a simple consequence of growth instabilities and aggregation processes driven by cohesive forces. One finds many examples everywhere: snowflakes, the spatial distributions in bacterial colonies, patterns formed by streams and river meanders, neuron cell networks, and mineral stones [3]–[8]. We could get a nice vivid picture of this phenomenon if we were to write and run a computer program based on a diffusion limited aggregation algorithm (DLA), which successfully describes dendritic growth in an ideal system [9].

However, one must be aware that the DLA is an algorithm designed to describe the aggregation phenomena under specific physical conditions, namely, in the limit of low particle concentration and slow aggregation. The DLA provides, under such conditions, a suitable description of the so called Laplacian growth, which can be considered a limit law. Of course, one cannot expect that the DLA will be able to describe aggregation phenomena where magnetic and hydrodynamic interactions, depletion forces, and a highly dissipative regime are present. Hence, depending on the characteristic times of the involved interactions, the dynamics of the aggregation could exhibit different degrees of complexity. The latter is the situation in which the dendritic growth we analyze here occurs [10]–[13].

The aggregation of magnetic particles is a physical phenomenon that has been studied in small systems like colloidal ones [14, 15] or large systems with small particles [16]. For example, experimental studies of irreversible aggregation in granular materials with long-range magnetic interactions have revealed a rich number of phase transitions and patterns: dense clusters, loose chains and rings [17, 18]. Here, the formation of dendrites is explored in a system where not only a competition between magnetic and inertial forces exists but where the aggregation, induced by a nucleation seed, is finite. The complex structures of

doi:10.1088/1742-5468/2013/12/P12015

J. Stat. Mech. (2013) P12015

many physical and mathematical sets have been studied in terms of their characteristic correlations. In this sense, some measures of the complexity in terms of the scaling relations coexisting in the structure have been proposed [19]. A detailed investigation of the behavior of the singularity spectrum for different sets has been analyzed in terms of DLA fluctuations [20]. For clusters formed by a much larger number of magnetic particles under the influence of an external drift, or under the influence of external fields, their multifractal properties in terms of their singularity spectrum have been discussed [21].

Our system is a driven granular gas composed of paramagnetic and glass beads randomly moving around a nucleation point (a magnetic sphere located below the base of the container). Hence, it is the dipole–dipole interaction between this nucleation point and the paramagnetic particles of the gas that induces the aggregation. Of course, there is a competition between magnetic and inertial forces in the formation of the clusters and, therefore, a diversity of finite dense clusters is obtained. Under the appropriate conditions, we observed tip, tip-split and side-branching growth.

These structures are classified into a phase diagram as a function of bead concentration and granular temperature. Many of the structures are quite similar to clusters generated by the diffusion limited aggregation algorithm (DLA), although with an important difference: there are, in our case, at least two well differentiated stages in the growing process of the agglomerates. These stages can be quantitatively characterized by means of two radial mass scaling relations. Moreover, in our system, we observe the evolution of clusters particle by particle; therefore, the aggregation time is easily measured. We find an exponential function that describes the aggregation phenomenon as a function of time, which is independent of the morphology (shape and length) of the structure. The existence of two or more scaling relations related to the clusters' growing regimes has been discussed for clusters numerically generated and for clusters grown physically, imposing different physical conditions [22, 23]. However, as we discuss below, the finite cluster growth size is a particular characteristic of the kind of central forces investigated here. This introduces novel aspects in the discussion of aggregation phenomena.

2. Experimental details and results

The experimental setup used in this work is depicted in figure 1(a). The granular system is a mix of steel and glass particles inside an acrylic 15 cm × 15 cm × 3 cm closed container fixed to a shaker. The numbers of particles used in our experiments are 530 to 2120 steel spheres ($D = 1.61$ mm, $m = 0.017$ g) and 350 to 2100 glass particles ($D = 2$ mm, $m = 0.0074$ g). The glass particles are used to incorporate additional stochasticity and recover equilibrium properties of ergodicity and a detailed balance, where the underlying chaotic dynamics serves as a thermal bath [24].

We define ϕ as the number of paramagnetic particles n_{p} divided by the number of glass particles n_g. The measured acceleration of the cell relative to gravity g is quantified by the parameter $\Gamma = (A\omega^2)/g$, where A and ω are the amplitude and frequency of the vibration. Γ was varied from 1.86 to 2.74. The dipolar magnetic interaction between the steel particles was induced by placing a magnetic dipole ($D = 5$ mm) centered underneath the base of the cell, see figure 1(b). The magnetic field strength of this dipole is $M = 12$ kG and the dipole moment is set to be perpendicular to the base. However, the field intensity measured above the acrylic base is around 400 G. In figure 1(c) we show how this intensity

J. Stat. Mech. (2013) P12015

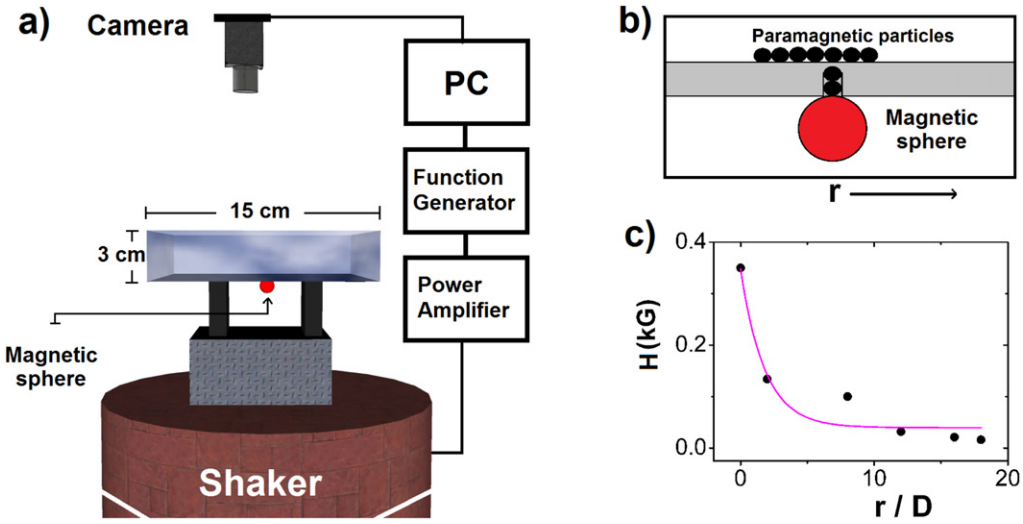

Figure 1. (a) A schematic diagram of the experimental apparatus. The red sphere represents the magnetic NdFeB ball. The shaker is driven by a power amplifier and the driving signal originates from a wave generator. Image data are acquired from the top by a digital camera. (b) A zoom of the zone where the magnetic sphere is located underneath the base of the cell. Note that there are two paramagnetic small beads incrusted inside the acrylic base. (c) The measured field intensity B as a function of r in a given chain of paramagnetic beads. Note that B decreases exponentially.

decreases as a function of the distance. The process of pattern formation is filmed with a digital camera (Pixelink PL-B742V) at 1 fps.

Our experiments begin with the creation of a granular gas (paramagnetic and glass particles) at a particular ϕ and Γ. In the absence of the magnetic dipole the particles are free and randomly dispersed. When the dipole is placed under the base, a non-trivial competition between the anisotropic magnetic potential and mechanic dissipative forces determines the structure of the emerging pattern. As we expect, the formation of chain configurations radially growing around the dipole is observed. Normally, magnetic chains are the most stable states, as observed by [17, 18]. Only when Γ is low and the number of glass particles high ($\phi < 1$) is the mechanism of growth forming tips predominant. A high number of glass beads produces a large number of collisions, screening the paramagnetic particles from reaching the cluster. This means that the paramagnetic particles need to explore the entire phase diagram to attach to the energetically most favorable state (the head–tail alignment, see figure 2(a)). For greater values of Γ and ϕ, the tip-split and dendritic growth appear during the aggregation process. We observe that lateral aggregation is ubiquitous, see figure 2. The dendritic growth starts when particles attach to robust (thick) chains, see figure 2(b). Under these conditions, tip splitting occurs in single chains (i.e. bifurcation occurs as observed in figure 2(c)).

The aggregation process that gives rise to the dendritic structure seems to be composed by at least two stages. In the first one, the aggregation of particles is faster, forming around the seed an apparently frozen compact region. Depending on the value of the parameters ϕ and Γ a structure is more or less compact. This is a stage where the magnetic

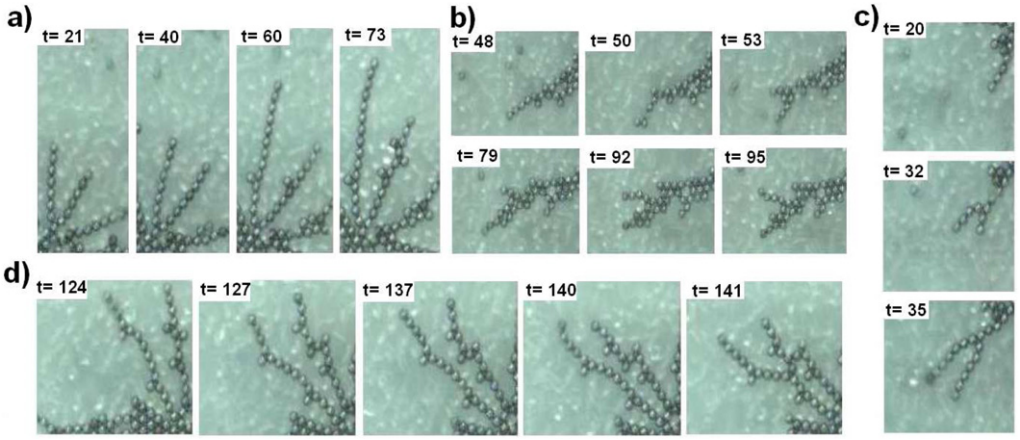

Figure 2. We show several image sequences of the cluster growth at $\phi = 0.3$ and $\Gamma = 1.86$. (a) Shows the lateral aggregation and the side-branching growth of a robust chain, (b) shows a typical tip growth and (c) shows tip splitting growth of a single chain. Finally, (d) shows aggregation of branches (time is shown in seconds). The position of the dipole (i.e. the seed) is outside the images: in ((a)-(c)) the dipole is in the opposite direction from the radial growth, in (d) the dipole is located in the direction of the right bottom corner.

interaction is clearly most relevant in the aggregation dynamics, although a dragging effect due to the collisions with the glass particles produces some rearrangement of the particles not attached with the strongest bonding. A second aggregation stage is observed with a different radial mass scaling. First-generation structures (tips and branches) merge due to an effective dipolar potential. As a matter of fact, if the lateral extremes of two branches connect, a new one is formed, see figure 2(d) at $t = 141$ s. Depending of the final shape of the structure, we can separate the aggregates into three distinctive groups: the dendrites group (figures 3(a)–(c)), the jellyfish-shaped group where quasi-3D structures are observed (figures 3(d)–(e)), and the flat jellyfish group with no 3D structures whatsoever (figures 3(f)–(h)). It is important to remark that the aggregates always remain tied to the bottom of the container. Obviously, this is due to the strong magnetic interaction between the seed and the first particles inside the container that become bound to it. At advanced stages of the aggregation process also the mass of the aggregate contributes to hold the cluster at the bottom of the container. The color contrast between the glass (transparent) and the paramagnetic particles (dark gray) allows us to observe, step by step, the aggregation process.

Let us describe in detail the final states of such patterns. When both ϕ and Γ are small, we observe the formation of simple dendrites with many branches (figure 3(a)). Complex dendrites are observed when branches give rise to splits (figure 3(b)). At high values of Γ, short branches and small fingers grow at the interface line (figure 3(c)). At high values of ϕ and Γ, quasi-3D jellyfish structures are observed. Here, small tips grow at the interface line and, depending of the number of glass particles, these may undergo dynamic arrest (figures 3(d)–(e)). Under the appropriate physical conditions, this arrest is observed when the lateral end of a branch is able to connect with another, forming a sort of corral where a central area with voids is established. During this process free glass

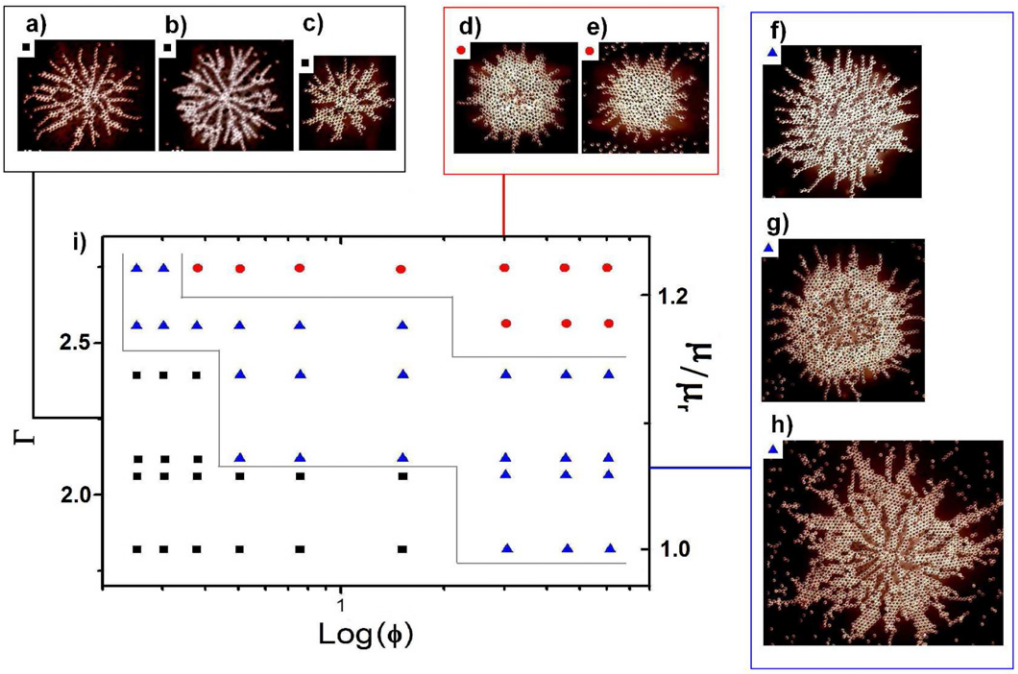

Figure 3. A diversity of dense clusters as a function of ϕ and Γ. In general, the most notable differences between the structures lie in the distribution of holes, the shape of their arms and tips and the degree of order. Only 20% of the structures are quasi-3D, corresponding to (e) and (d). (a)–(c) Show clusters generated at $\phi = 0.3$ and $\Gamma = 1.86$, 2.06 and 2.12, respectively, see black squares; (d) and (e) show clusters generated at high ϕ and Γ ($\phi = 3$ and 4.5 and $\Gamma = 2.56$ and 2.74 respectively), see red dots; (f)–(h) show aggregates generated at high ϕ and low Γ ($\phi = 3$, 4.5 and 6 and $\Gamma = 1.86$, 2.06 and 1.86 respectively), see blue triangles; (i) shows the full morphology diagram. The vertical scale on the right is the ratio of the magnetic moment of the beads at a given Γ relative to the magnetic moment μ_r at $\Gamma = 1.86$. With this scale we can see that the higher the value of Γ the greater μ is needed to hold the beads on the tips.

particles can be trapped inside this corral (figures 3(f)–(h)). If the collisions in this area are sufficiently energetic, the particles can deform the chains and reorder the structure. Figure 3(i) shows the phase diagram of the clusters as a function of ϕ and Γ. The way in which a drift externally imposed affects the aggregation processes has been investigated in several systems and under several conditions [21, 25, 26]. As expected in our case, with the dipole of the seed perpendicular to the bottom of the container, the drift caused by the glass beads and the magnetic interaction generates clusters with azimuthal symmetry.

3. Analysis and discussion

The pattern complexity of the structures shown in figure 3 can be characterized by their mass fractal dimension, the radial scaling of mass, and the radial distribution function. The mass fractal dimension is defined by the power law: $m \propto r^d$ where m is the mass contained in a circle of radius r. To find d, using the digital images of the clusters, it is

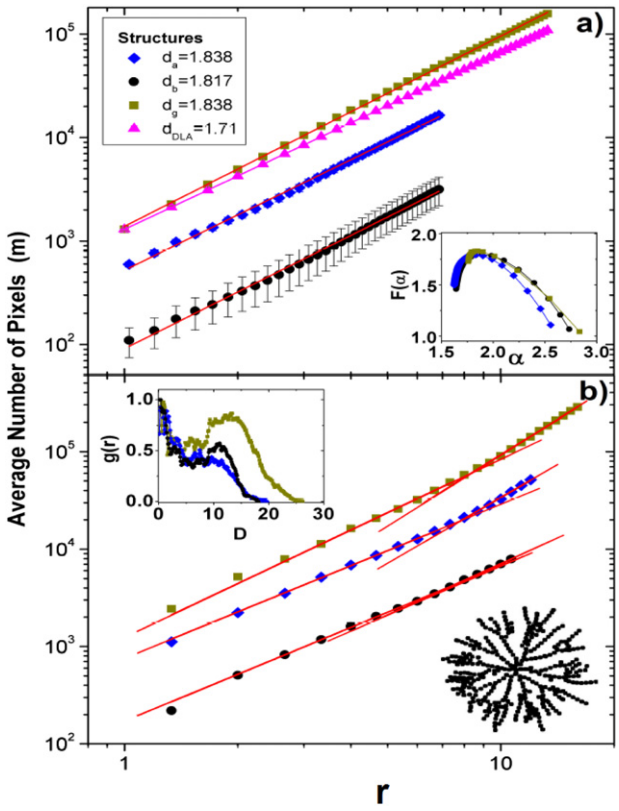

Figure 4. (a) Log–log graph of the average number of pixels (m) associated to the paramagnetic particles versus the gyration radius r taken at different sites of the structure (for clusters (a), (b), and (g) of figure 3). The points are the average of ten measurements and the error bars the standard deviations. The slope of the fitted straight lines is the corresponding mass fractal dimension. The lines were separated by a constant to appreciate their differences. Inset: the singularity spectrum of these objects $F(\alpha)$ versus α indicates that they are fractal. The maximum value of the curve corresponds approximately to the fractal dimension. (b) Log–log graph of the average number of pixels (m) associated to the paramagnetic particles versus the gyration radius r taken from the center of the structure (for clusters (a), (b), and (g) of figure 3). The slopes of the lines are $\xi_a = 1.58; 2.23$, $\xi_b = 1.61; 1.73$ and $\xi_g = 1.63; 2.40$. The lines were separated by a constant to appreciate their differences. Insets: the radial distribution of mass for such structures and the structure of figure 3(b) after the high-contrast treatment.

necessary to make first a high-contrast treatment of each image in order to define a single plane in the structure (see for example the lower inset of figure 4(b), which corresponds to figure 3(b)). The analysis of all the structures is carried out on the same plane which corresponds to the deepest layer of the aggregate (the one that touches the bottom of the cell). To define this plane, the photographs of aggregates were transformed to grayscale, the brightness and threshold were changed, and, finally, transformed to a binary scale.

Afterwards, we numerically draw a number of equally separated concentric circles, starting with a small one (of the order of the particle diameter) up to circles as large as the diameter of the cluster. The number of pixels found in an element area is proportional

J. Stat. Mech. (2013) P12015

to the mass contained in the same element. This procedure is repeated by drawing sets of concentric circles at several different sites (centers) of the structure and for several structures formed under the same physical conditions. To avoid the effects of small local inhomogeneities and to mainly capture the trends and correlations of the global structure statistically, the average of the number of pixels obtained was calculated for the corresponding circles for all sites in the structure. The reproducibility of our experiments is reasonable, in the sense that, under the same physical conditions, the final general shape and size of the aggregates is the same. We have measured the mass fractal dimension in a large number of aggregates grown under the same conditions and found values very similar for each structure. Then, due to the aforementioned reproducibility, the quantities reported are the average of the measurements from three structures. The mass fractal dimension has proven to be a useful tool to characterize a great diversity of two-dimensional structures [27]. In order to compare the structural characteristics of the clusters shown in figures 3(a)–(h) to those grown by a DLA algorithm, we have estimated a fractal dimension by finding the maximum value of the singularity spectrum $F(\alpha)$ versus α of these objects [28]. We used Fraclac (a plugin of ImageJ) to estimate these fractal dimensions defined as

$$F(\alpha) = \frac{\sum_i \mu_i \log \mu_i}{\log(\epsilon)}, \tag{1}$$

where $\alpha = (\sum_i \mu_i \log P_i)/\log(\epsilon)$ and $\mu_i = P_i^Q / \sum_i P_i^Q$, where P_i is the probability to find pixels in the ith box and Q a parameter that goes from -10 and 10. The maximum value of the singularity spectrum is the fractal dimension of a structure. We found that $d_a^{\mathrm{s}} = 1.80 \pm 0.001$, $d_b^{\mathrm{s}} = 1.83 \pm 0.006$, $d_c^{\mathrm{s}} = 1.87 \pm 0.015$, $d_{\mathrm{d}}^{\mathrm{s}} = 1.82 \pm 0.011$, $d_e^{\mathrm{s}} = 1.84 \pm 0.010$, $d_f^{\mathrm{s}} = 1.83 \pm 0.007$, $d_g^{\mathrm{s}} = 1.85 \pm 0.003$ and $d_h^{\mathrm{s}} = 1.81 \pm 0.008$. Note that these dimensions differ from those obtained by the DLA ($d_{\mathrm{DLA}} = 1.71$).

Furthermore, we found that the mass scales with the radius (measured from the position of the seed), with two distinctive power laws indicating that there are two stages in the aggregation process by which the hierarchical structure of the system is formed. A detailed analysis has been made for DLA clusters generated under different conditions [22, 29]. For those clusters, the appearance of a crossover in the effective fractal dimension when they reach a certain threshold size has been discussed. Of course, there are important differences between the clusters analyzed here and the DLA ones. This is why the properties of clusters formed by means of a 2D DLA algorithm must be understood only as a reference, because in our case the quasi-2D structures are the result of the aggregation of particles moving in a semi-quasi-3D space. In other words, the present setup establishes, from the beginning, different conditions from those in which the DLA is valid. Nevertheless, we performed additional experiments in which the paramagnetic particles were introduced one by one inside the cell with the gas of glass beads, similarly to how the DLA algorithm works. This to confirm that the aggregates were of the same shape as the ones described in this paper (where the steel and glass particles were introduced together in the cell before the vibrations).

In our case, the appearance of the crossover in the mass radial scaling seems to merge when the cluster size reaches a value at which the magnetic interaction begins to be significatively counteracted by the drift produced by the glass particles, and consequently becomes unable to hold a dense structure (even though it continues growing by forming

chains). The change of the aggregation regime could be also recognized as a slight kink in the straight lines fitted to the average number of pixels as a function of the gyration radius, i.e., in the value of the mass fractal dimension. However, because of the relatively small number of particles integrating the clusters, the corresponding fluctuations in the pixel number are too large to be a reliable determination of a change in the mass fractal dimension. Clusters formed by a larger number of paramagnetic particles, smaller than ours, whose structures exhibit more than one regime in their aggregation processes and more than a single mass fractal dimension, have been studied with a similar method in magnetorheological dispersions in the presence of external magnetic fields [27].

The use of the term fractal, for physical objects, must be taken with care. In the so called physical fractals, the concept of scale-free behavior has clear limitations. This is why instead of self-similarity one needs to refer to self-affinity. In refinement procedures of physical fractals, it must be understood that self-affinity is obtained as a statistical-wise characteristic and for a finite number of spatial scale changes.

For a 2D object, the mass radial distribution can be written in the form

$$g(r) = \frac{M(r+\Delta) - M(r)}{\pi[(r+\Delta)^2 - r^2]}, \tag{2}$$

where $M(r)$ is the mass contained in a circle of radius r and Δ is a small increment in r, or, equivalently, the separation between two contiguous circles. Clearly, in our system, this quantity can give information about the profiles of the mass distribution from the center of the aggregates to the border. The upper inset of figure 4(b) shows $g(r)$ for the structures corresponding to the ones discussed in figure 3(a). The mass distribution reaches its maximum value somewhere in the inner region of the structures and then descends to zero. For a given value of Γ, an obvious decreasing behavior of the mass distribution must start at those values of r where the magnetic interaction is becoming relatively weak, namely, at the periphery of the dense and almost frozen region, where tips start growing. However, for shorter values of r also the behavior of the mass radial scaling has an interesting structure. Figure 4(b) shows the mass radial scaling measured from the center of the cluster up to values of r where the tips start growing, for the agglomerates (a), (b), and (g) of figure 3. The error bars are as large as the size of the symbols. Clearly, the curves exhibit two well differentiated segments that can be well fitted by straight lines with different slopes. Note that these slopes do not represent the mass fractal dimension. The three curves exhibit a crossover between two regimes of mass radial scaling in the inner frozen region of the corresponding cluster. The existence of these aggregation regimes is more clearly observed for the dendritic structure (a) and the jellyfish clusters (g). In the case of structure (b) it is less clear.

An interesting question about the aggregation of the magnetic beads is the following: how fast is the process for a given value of Γ? This growing process can be followed by measuring the area spanned by the aggregated particles at different times. It requires a high-contrast treatment of the digital images of figure 5, easily carried out with the software ImageJ. We found that the area subtended by the structures, A_r, changes in time exponentially according to

$$A_r = A_{\mathrm{T}}(1 - \mathrm{e}^{-t/\tau}), \tag{3}$$

J. Stat. Mech. (2013) P12015

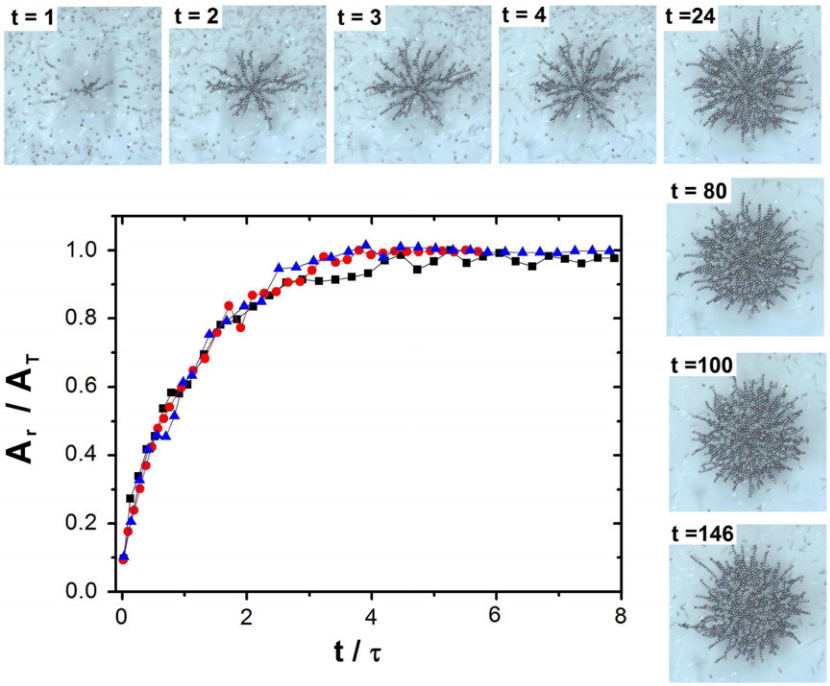

Figure 5. Rescaled area of the aggregates, A_r/A_T versus t/τ for $\phi = 0.3$, 0.5 and 1.5 at $\Gamma = 2.12$. The curves display a universal scaling. A sequence of structures obtained for $\phi = 1.5$ and $\Gamma = 2.12$ is also shown (time is shown in seconds).

where τ is a characteristic time interval of the aggregation. During this interval, the dominant magnetic interaction generates the compact zone of the structure. τ is also roughly related to the change in time of the mass scaling regime. In other words, it is a characteristic time at which the cluster reaches the mean radius where the magnetic interaction becomes weakened, producing the change in the regime of aggregation that is exhibited by the change in the mass radial scaling. A_T is the maximum area that a cluster can reach for the given values of ϕ and Γ. Figure 5 shows that the growth is independent of the final shape and length of the final structure. A similar result for the radius of gyration was obtained by other authors [17, 18].

Now, in order to say few words about how a dendritic structure forms let us introduce a parameter λ. This parameter compares two energies that compete with each other: the dipole–dipole interaction energy E_d, mainly for dipoles aligned head to tail, and the granular averaged thermal energy E_T. Thus,

$$\lambda = \frac{E_d}{E_T} = \frac{\mu^2 a^{-3}}{(1/2)m\langle v^2\rangle}, \tag{4}$$

where m and a are the mass and particle radius and μ the magnetic moment of a given particle. Since E_T is proportional to Γ [17], we can obtain a simple expression for λ:

$$\lambda = \frac{\mu^2 a^{-3}}{\alpha\Gamma} \tag{5}$$

where α is a proportionality constant.

When the magnetic forces dominate over inertial ones, the aggregation occurs fast near the point where the magnetic seed is located. In this case, $\lambda > 1$. When the farthest beads of the structure are in equilibrium with the gas $\lambda \leq 1$. Thus, an expression for the minimum value of the local magnetic moment, capable of holding a magnetic particle to the cluster, is found when $\lambda = 1$, and is clearly a function of Γ (see the right scale of figure 3(i)):

$$\mu = \left(\alpha \Gamma a^3\right)^{1/2}. \tag{6}$$

One could expect that this value for the local minimum magnetic moment would be well defined in an ideal crystalline cluster. This condition, $\lambda = 1$, is related to a cluster size at which, except for small fluctuations, the magnetic interaction is unable to hold tips growing on the peripheral region of the circular cluster. However, as is shown in figure 3 and 5, the clusters are nonhomogeneous structures. In fact, the mass scaling with the cluster radius is statistically well described by a fractal dimension up to a certain threshold radius, and then the scaling changes. The defects, impurities, and lacunae of the cluster structure, as well as the stochastic fluctuations of the collisions with the glass particles, mean that at the peripheral region of the cluster magnetic potential minima still exist (capable of bonding particles in the tail–head configuration), generating in this way growing tips.

The density and lacunarity characteristics of DLA structures have been investigated by measuring the angular distribution of main arms as a function of the number of aggregated particles [29, 30]. Most of the theoretical growing models so far proposed as extensions, or based on DLA, to analyze multifractality [19, 20], drift effects [25, 26], self-similarity deviations [22, 29], and kinetic lattice models [23] agree in the prediction of a crossover in the regime of growth between a frozen compact region with no further activity, a regime characterized by a scaling relation between the mass and the gyration radius, and at least one still active and less compact region characterized by a different scaling relation. However, some physical differences between the growing conditions of our clusters make inappropriate a direct comparison between the values of the respective fractal dimensions. Some of them are the following: (a) the small number of aggregated particles in our experiments, (b) the anisotropy introduced by the drift (in our case the drift caused by the glass particles on the clusters cannot be considered isotropic), and (c) the finite range of the magnetic interaction, which means that the clusters reach, in turn, a finite size. Of course, this latter consideration does not mean that the changes in the mass radial scaling in the different growth regimes and the existence of the crossover are simply due to the fact that the physical interaction dominating the growth changes. We believe it is not as simple as this. There are complex factors that contribute to this change in the scaling. For instance, the symmetry and quasidimensionality of the space play an important role. The fact that the whole structure of the cluster evolves continuously from the beginning means that the drift effect produced by the glass particles, which move in a quasi-3D space and affect the 2D structure of the clusters, has an important role.

The results shown in figure 5 indicate that, as result of the drift, the dense central region of the aggregates evolves in time, reducing the lacunae area. This is another fundamental difference in what occurs with 2D clusters generated by the DLA and some other algorithms as well. In these, the arrangements of particles in an inner region of a lacuna, once this has formed, do not change because the drift does not have access to it.

J. Stat. Mech. (2013) P12015

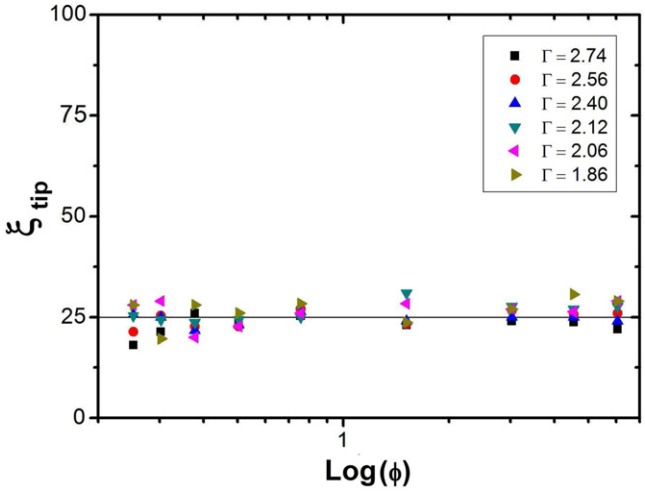

Figure 6. ξ_{tip} versus ϕ for the final structures observed in our experiment. The average of ξ_{tip} is almost insensitive to the final shape and the length of the structure.

In other words, the drift modifies the outer structure of the cluster but does not affect the inner [25, 26]. Indeed, the general shape of these magnetic clusters, namely, a dense structure ended by a corona, resembles those generated by means of the Eden model [23], rather than the DLA.

We measured the number of tips ξ_{tip} as a function of ϕ and Γ and calculated its mean value for the three different aggregates generated with the same physical conditions (same parameters). This was carried out using images of the final structure. As we can see in figure 6, $\langle \xi_{\mathrm{tip}} \rangle$ is around 25 for all the structures, probably revealing that this dendrite saturation limit is reached in the first stage of the growth and scales with the magnetic seed strength. Maybe the last aggregation step of forming tips can be understood by thinking that in this regime both magnetic field bonding and bead concentration in the surrounding space have decreased. In these conditions, the aggregation of beads forming chains is the way to reduce free energy and increase entropy [31].

4. Conclusions

We studied the aggregation of paramagnetic particles around a magnetic seed and found a dynamics characterized by two scaling relations, where tip, tip-split and branch merging are observed. Since the beads do not have a permanent dipole moment and the growth is induced by a nucleation point, mass starts to fill the central region of the structure by the diffusion of particles from the gas, forming jellyfish-like bodies. Moreover, branches collapse into each other due to an effective magnetic interaction. This branch merging seems to be a particular feature of the system here investigated, and this is the mechanism which originates the lacunae in the frozen region making the clusters fractal objects. Yet, dendrites survive in the periphery of the structures as reminiscent of the first stage of growth. An exponential function describes the evolution of the agglomerates which is independent of the morphology of the structures.

As far as we know, this work is the first experimental study where a dendritic growth is observed in real time, particle by particle, and with the naked eye.

Acknowledgments

This work has been supported by Conacyt, Mexico, under grants 101384 and 104616, and VIEP-BUAP grant CAEJ-EXC11-1. JGG acknowledges a fellowship from CONACyT.

References

[1] Burd A B and Jackson G A, 2009 *Annu. Rev. Mar. Sci.* **1** 65
[2] Meakin P, 1988 *Annu. Rev. Phys. Chern.* **39** 237
[3] Westbrook C D, Ball R C and Field P R, 2004 *Geophys. Res. Lett.* **31** 15104
[4] Ben-Jacob E, Shochet O, Tenenbaum A, Cohen I, Czirók A and Vicsek T, 1994 *Nature* **368** 46
[5] Matsushita M and Fujikawa H, 1990 *Physica* A **168** 498
[6] London M and Hausser M, 2005 *Annu. Rev. Neurosci.* **28** 503
[7] Schumm S A, 1985 *Annu. Rev. Earth Planet. Sci.* **13** 5
[8] Chopard B, Herrmann H J and Vicsek T, 1991 *Nature* **353** 409
[9] Witten T A Jr and Sander L M, 1981 *Phys. Rev. Lett.* **47** 1400
[10] Ben-Jacob E, Coffey D S and Levine H, 2012 *Trends Microbiol.* **20** 403
[11] Yuya O and Imai I H, 2003 *Cryst. Growth Des.* **3** 711
[12] Kramer S and Marder M, 1992 *Phys. Rev. Lett.* **68** 205
[13] Chopard B, Herrmann H J and Vicsek T, 1991 *Nature* **353** 409
[14] Patel R and Chudasama B, 2009 *Phys. Rev.* E **80** 012401
[15] Snezhko A and Aranson I S, 2007 *Phys. Lett.* A **363** 337
[16] Ostriker J P, 1993 *Annu. Rev. Astron. Astrophys.* **31** 689
[17] Blair D L and Kudrolli A, 2003 *Phys. Rev.* E **67** 021302
[18] Snezhko A, Aranson I S and Kwok W K, 2005 *Phys. Rev. Lett.* **94** 108002
[19] Halsey T C, Jensen M H, Kadanof L P, Procaccia I and Shraiman B I, 1988 *Phys. Rev.* A **33** 1141
[20] Halsey T C, Duplantier B and Honda K, 1997 *Phys. Rev. Lett.* **78** 1719
[21] Mora E C, Carrillo J L, Mendoza M E and Donado F, 2013 *Eur. Phys. J.* B **86** 1
[22] Mandelbrot B B, Kaufman H, Vespignani A, Yekutieli I and Lam C H, 1995 *Europhys. Lett.* **29** 599
[23] Ausloss M, Vandewalle N and Cloots R, 1993 *Europhys. Lett.* **24** 629
[24] Egolf D A, 2000 *Science* **287** 101
[25] Meakin P, 1983 *Phys. Rev.* B **28** 5221
[26] Nagatani T, 1988 *Phys. Rev.* A **37** 3514
Nagatani T, 1989 *Phys. Rev.* A **39** 438
[27] Carrillo J L, Donado F and Mendoza M E, 2003 *Phys. Rev.* E **6** 061509
Carrillo J L, Mendoza M E and Donado F, 2005 *J. Stat. Mech.* P06001
[28] Chhabra A and Jensen R V, 1988 *Phys. Rev. Lett.* **62** 1327
[29] Mandelbrot B B, Kol B and Aharony A, 2002 *Phys. Rev. Lett.* **88** 055501
[30] Allain C and Cloitre M, 1991 *Phys. Rev.* A **44** 3552
[31] Levin Y, 2002 *J. Phys.: Condens. Matter* **14** 2303